NJC

PAPER

View Article Online
View Journal

Cite this: DOI: 10.1039/c6nj01314g

Novel D–π–A type triphenylamine based chromogens for DSSC: design, synthesis and performance studies†

Behzad Hosseinzadeh,[a] Alireza Salimi Beni,*[b] Masoumeh Azari,[b] Maryam Zarandi[b] and Marzeih Karami[b]

Received (in Montpellier, France) 25th April 2016,
Accepted 27th July 2016

DOI: 10.1039/c6nj01314g

www.rsc.org/njc

In this work, four novel D–π–A organic dyes (**MH**, **MT**, **DT**, **DH**) consisting of triphenylamine as an electron donor and 2,4-thiazolidinedione/hydantoin as anchoring groups were designed and synthesized for use in dye-sensitized solar cells (DSSCs). The synthesized dyes were characterized using FT-IR, NMR, mass spectrometry, absorbance and electrochemical measurements. The photophysical, electrochemical and photovoltaic properties of the solar cells based on these dyes were investigated to study the effect of two different anchoring groups on the performance of the dye-sensitized solar cells. The dye consisting of two hydantoin anchoring groups shows the highest conversion efficiency of 2.70% (short-circuit current = 7.60 mA cm^{-2}, open circuit voltage = 570 mV, and fill factor = 0.62 under standard AM1.5G irradiation) compared to the other designed dyes. The observed results will provide basic information for the future design of sensitizers with different anchoring groups for photovoltaic applications.

1. Introduction

In recent years, the quest for renewable energy has received worldwide attention owing to the fast depletion of fossil fuel reserves and the environmental pollution problems that accompany fossil fuel consumption. Solar energy conversion devices that convert sunlight into electricity are seen as inevitable future energy candidates due to the unlimited supply of solar energy.[1,2]

Dye-sensitized solar cells have been significantly developed as energy conversion devices, due to their competent performance and low production costs.[3–5] Dye-sensitized solar cells (DSSCs) are the most effective renewable photovoltaic devices because of their advantages such as ease of fabrication, short energy payback time, low sensitivity to temperature variation, flexibility, transparency, efficiency at different angles with low light intensity and low emission of CO_2, and also they are more environmentally friendly than conventional inorganic solar cells. Among the major components of DSSCs, the sensitizer plays a crucial role in achieving a high power conversion efficiency and has been extensively studied. To overcome the high cost of ruthenium complexes, metal free organic dyes have been extensively explored in recent years. For example, zinc porphyrins as dye containing metal have achieved a maximum power conversion efficiency of 13%.[6] Metal-free organic sensitizers have also shown promise due to their advantages such as low cost, high molar extinction coefficient, and facile molecular design. Recently, an unprecedented power conversion efficiency of 10.3% was reported for an organic sensitizer,[7] indicating that with further strategic optimization, metal-free organic sensitizers may overtake their organometallic counterparts in terms of photovoltaic performance. Novel organic sensitizers such as triarylamine,[8] coumarin,[9–11] tetrahydroquinoline,[12,13] merocyanine,[14,15] cyanine,[16,17] phenothiazine,[18] indoline,[19,20] and hemicyanine[21,22] have been used in DSSCs with good results. A typical structure of metal-free organic sensitizers is a donor–π-bridge–acceptor system (D–π–A). An appropriate donor will lead to a good light absorption spectrum and matched energy levels with both the conduction band edge of TiO_2 and the redox potential of the electrolyte. Therefore, the choice of a donor moiety and its structural optimization are critical to the spectral response, charge injection efficiency and stability of sensitizers with high photovoltaic performance. Among the various organic dyes, triphenylamine (TPA) is still one of the most popular donor moieties and the modification of TPA is desirable.[23–26] A successful approach has been demonstrated by incorporating a planar amine with bulky substituents, which not only could increase the charge-separated state lifetime by the delocalization of the generated cation over a planar amine unit but also could avoid dye aggregation.[27] With two adjacent phenyl rings connected by a methylene linker, bridged TPA is a

[a] Department of Chemistry, Mazandaran University, Babolsar, Iran
[b] Chemistry Department, Yasouj University, Yasouj 75918-74831, Iran. E-mail: salimibeni@mail.yu.ac.ir; Tel: +987412223028

† Electronic supplementary information (ESI) available. See DOI: 10.1039/c6nj01314g

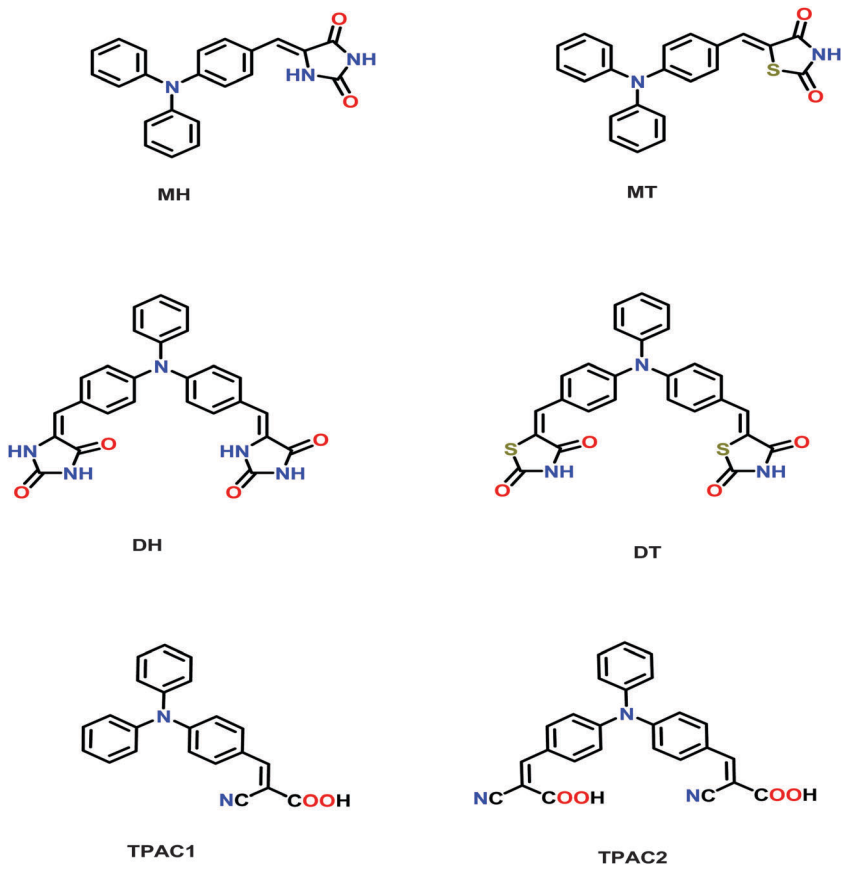

Fig. 1 Chemical structures of the reference compound **TPACn** and the triphenylamine based dyes **MH**, **MT**, **DH** and **DT**.

potential donor unit in constructing a donor–π–acceptor (D–π–A) type system.

It is notable that many academic groups have investigated metal-free sensitizers, but the design of sensitizers containing new anchoring groups is in its infancy and is one of the interesting points in the design of sensitizers.

In this study, in continuation of our investigation to develop new sensitizers and find novel anchoring groups for sensitizers,[28,29] four types of triphenylamine-based organic dyes **MH**, **MT**, **DH**, and **DT** (molecular structures are shown in Fig. 1) with two different anchoring groups were designed and synthesized as sensitizers for DSSCs. The acceptor/anchoring groups used are 2,4-thiazolidinedione and hydantoin. The photophysical, electrochemical, and photovoltaic properties of the dyes were also investigated.

2. Experimental section

2.1 Equipment and materials

^{1}H and ^{13}C NMR spectra were recorded on a Bruker 400 Ultrashield NMR and $CDCl_3$ or DMSO-d_6 was used as a solvent. FT-IR spectra were recorded in a KBr matrix using a JASCO FT-IR-680 plus spectrometer. Elemental analyses were performed using a Heraeus CHN–O-Rapid analyzer. Mass spectra of the products were obtained using a HP (Agilent technologies) 5937 Mass Selective Detector. Melting points were measured on an electrothermal KSB1N apparatus. Chemicals were purchased from Aldrich, Fluka and Merck chemical companies.

2.2 Synthesis and characterization of compounds

Scheme 1 shows the synthetic approach for the new chromophores **MH**, **MT**, **DH** and **DT**. These dyes were synthesized by well-known reactions such as the Vilsmeier–Haack formylation reaction and Knoevenagel reaction. The starting triphenylamine (TPA) was synthesized from phenylamine and iodobenzene in a nitrogen atmosphere (Cu catalyst, 115 °C, 3.5 h).[30] In the next step, compound **1** and **2** were synthesized *via* a Vilsmeier reaction. During the formylation reactions, the number of aldehyde groups introduced was controlled by varying the amount of $POCl_3$. Then, Knoevenagel condensation reactions of these aldehydes with 2,4-thiazolidinedione and hydantoin afforded the target dyes **MH**, **MT**, **DH** and **DT** in acetic acid using ammonium acetate as a catalyst.

2.3 General procedures for the synthesis of MH, MT, DH and DT

Aldehyde (1 mmol) and hydantoin or 2,4-thiazolidinedione (1.5 mmol) were added to 15 mL of glacial acetic acid and refluxed in the presence of 150 mg of ammonium acetate. After cooling to room temperature, the mixture was poured into ice water. The solid was filtered and washed with water. Finally, the

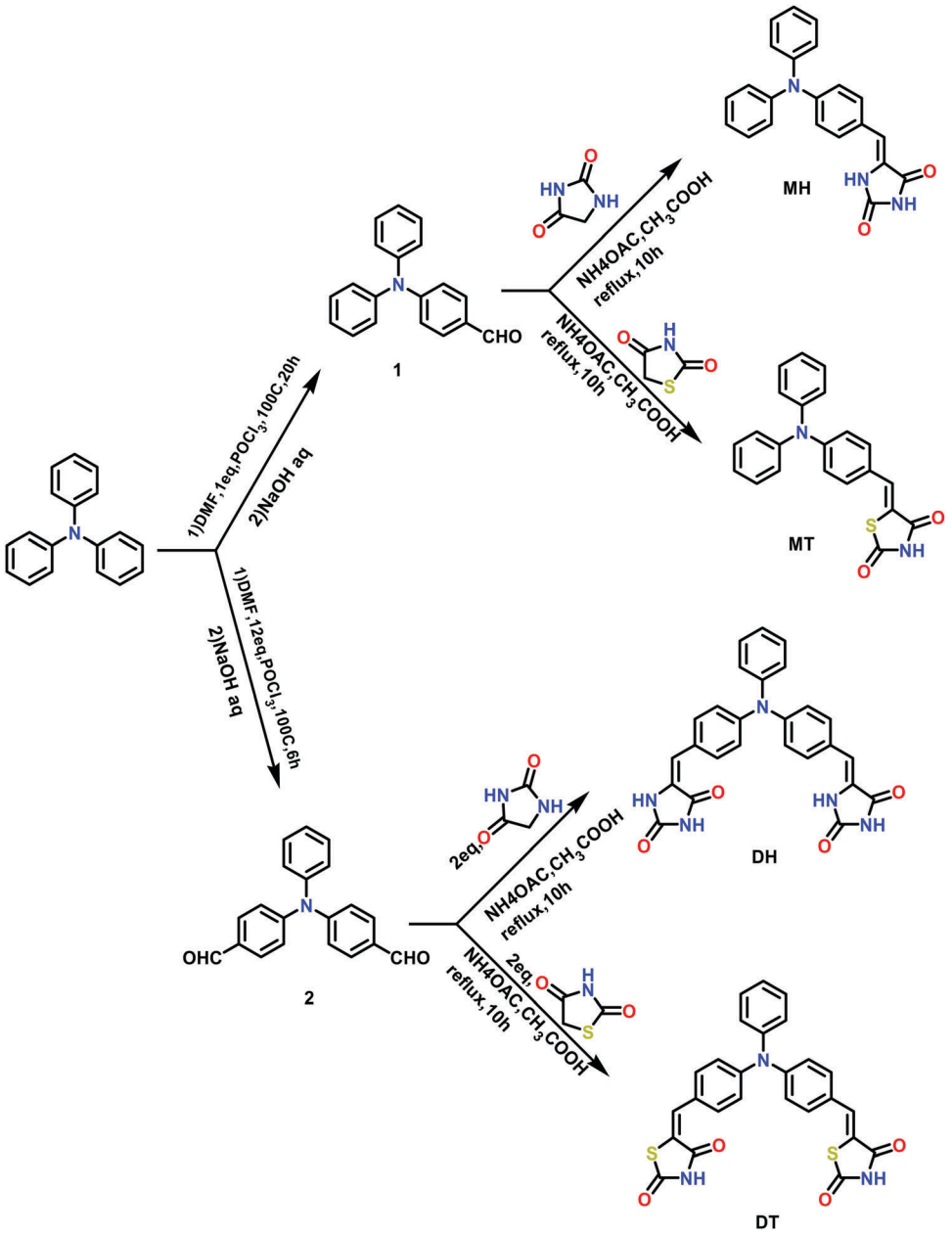

Scheme 1 Synthetic procedure of the organic dyes.

precipitate was purified by column chromatography (hexane/ethyl acetate).

2.3.1 Synthesis of 4-(diphenylamino) benzaldehyde (1). The synthesis of this compound was carried out based on a previously reported method.[31] To a mixture of Ph_3N (3 g, 12.23 mmol) and DMF (40 mL) at 0 °C was added $POCl_3$ (1.2 mL, 12.87 mmol, 1.05 eq.) dropwise with stirring. The resulting mixture was stirred at 95–100 °C under nitrogen for 20 h after which TLC analysis showed that no starting material remained. The mixture was then cooled to room temperature, poured into ice–water (150 mL) and neutralized with 4 M NaOH solution. The solid was collected, washed with water, dried, and purified by column chromatography on neutral alumina using a mixture of ethyl acetate/*n*-hexane (1 : 5, v/v) to give a pale yellow solid (yield = 94%). m.p.: 129–131 °C; FT-IR (cm^{-1}): 1690, 1492, 1335, 1308, 1229, 1157, cm^{-1}. Anal. cacld for $C_{19}H_{15}NO$: C, 83.49, H, 5.53, N, 5.13. ^1H NMR ($CDCl_3$-d_6, 400 MHz): δ (ppm): 9.82 (s, 1H, CHO), 7.70 (d, J = 8.7 Hz, 2H), 7.36 (t, J = 7.7–8.2 Hz, 4H), 7.21–7.17 (m, 6H), 7.04 (d, J = 8.7 Hz, 2H); ^{13}C NMR ($CDCl_3$-d_6, 100 MHz): 189.94, 153.32, 146.58, 132.45, 130.89, 129.37, 127.51, 126.25, 120.54; anal. calcd for $C_{19}H_{15}NO$: C, 83.49, H, 5.53, N, 5.13. Found: C, 83.49, H, 5.57, N, 5.15.

2.3.2 Synthesis of 4,4′-(phenylazanediyl)dibenzaldehyde (2). Compound **2** was prepared using a previously reported method.[32] To a mixture of Ph_3N (1 g, 4.08 mmol) and DMF (8 mL) at 0 °C was added $POCl_3$ (4 mL, 42.91 mmol, 10.5 eq.) dropwise with stirring.

The resulting mixture was stirred at 95–100 °C under nitrogen for 6 h, followed by similar workup, and purified by column chromatography (silica gel, EtOAc–hexane 1 : 4, v/v) to give a yellow solid (yield = 71%). m.p. 141–143 °C; FT-IR (cm^{-1}): 1703, 1591, 1512, 1499, 1335, 1295, 1223, 1177, 834. ^{1}H NMR ($CDCl_3$-d_6, 400 MHz): δ (ppm): 9.85 (s, 2H, CHO), 7.77 (d, J = 8.7 Hz, 4H), 7.41 (t, J = 7.6–8.0 Hz, 2H), 7.30 (m, 1H), 7.22–7.19 (m, 2H), 7.20 (d, J = 8.6 Hz, 4H); ^{13}C NMR ($CDCl_3$-d_6, 100 MHz): 190.88, 152.42, 145.82, 131.69, 130.55, 127.16, 127.51, 126.86, 123.64, anal. calcd for $C_{20}H_{15}NO_2$: C, 79.71, H, 5.02, N, 4.65. Found: C, 79.63, H, 5.07, N, 4.63.

2.3.3 Synthesis of 5-[(*Z*)-1-(4-diphenylaminophenyl)methylidene]-2,4-imidazolidinedione (MH). The synthesis of this compound was carried out based on general procedures, giving a pale yellow solid (yield = 85%); m.p. = 209–211 °C; FT-IR (cm^{-1}): 3426, 3192, 1746, 1713, 1648, 1588, 1510, 1490, 1383, 1285, 1177, 1097, 1017, 879, 754, 696, 543; ^{1}H NMR ($CDCl_3$-d_6, 400 MHz): δ (ppm): 8.55 (s, 1H), 8.43 (s, 1H), 7.27–7.34 (m, 6H), 7.10–7.16 (m, 6H), 7. 05 (d, J = 8.8 Hz, 2H), 6.67 (s, 1H). ^{13}C NMR ($CDCl_3$-d_6, 100 MHz): 164.4, 154.7, 148.9, 146.7, 130.3, 129.6, 125.5, 124.8, 124.2, 121.8, 112.9. Mass: m/z 355 (M + 1), 283, 180, 77. Anal. calcd for $C_{22}H_{17}N_3O_2$: C 74.35, H 4.82, N 11.82, O 9.00; found: C 74.30, H 4.80, N 11.79, O 8.96.

2.3.4 Synthesis of 5-[(*Z*)-1-(4-diphenylaminophenyl)methylidene]-1,3-thiazolane-2,4-dione (MT). The synthesis of this compound was carried out based on general procedures, giving an orange solid (yield = 87%); m.p. 270–272 °C; FT-IR (cm^{-1}): 3466, 3181, 1736, 1685, 1582, 1506, 1490, 1329, 1285, 1192, 754, 695, 641. ^{1}H NMR ($CDCl_3$-d_6, 400 MHz): δ (ppm): 9.21 (s, 1 H), 7.81 (s, 1 H), 7.33–7.37 (m, 6H), 7.15–7.19 (m, 6H), 7.05 (d, J = 8.8 Hz, 2H). ^{13}C NMR ($CDCl_3$-d_6, 100 MHz): 167.7, 167.2, 150.3, 146.3, 134.5, 131.9, 129.7, 126.0, 125.0, 124.8, 120.5, 118.0. Mass: m/z = 372 (M + 1), 355, 301; anal. calcd for $C_{22}H_{16}N_2O_2S$: C 70.95, H 4.33, N 7.52, O 8.59, S 8.61; found: C 70.91, H 4.31, N 7.50, O 8.56, S 8.59.

2.3.5 Synthesis of 5-((*Z*)-1-{4-[4-(2,5-dioxotetrahydro-1*H*-4-imidazolylidenmethyl)(phenyl)anilino]phenyl}methylidene) 2,4-imidazolidinedione (DH). Same as the general procedure but 4,4′-(phenylazanediyl)dibenzaldehyde (301 mg, 1 mmol) instead of 4-(diphenylamino)benzaldehyde and hydantoin (300 mg, 3.0 mmol) was used. The isolated yellow solid is **DH**, yield: 82%, m.p. 215–217 °C. FT-IR (cm^{-1}): 3423, 1755, 1717, 1651, 1590, 1509, 1389, 1299, 1185, 878, 835, 698. ^{1}H NMR (DMSO-d_6, 400 MHz): δ (ppm): 11.20 (s, 2H), 10.47 (s, 2H), 7.55 (d, J = 8.0 Hz, 4H), 7.37 (t, J = 8.0 Hz, 2H), 7.16 (t, J = 8.0 Hz, 1H), 7.10 (d, J = 8.0 Hz, 2H), 6.97 (d, J = 8.0 Hz, 4H), 6.37 (s, 2H). ^{13}C NMR (DMSO-d_6, 100 MHz): 166.0, 156.1, 147.1, 146.5, 131.3, 130.4, 127.9, 127.1, 126.0, 125.1, 123.4, 108.6. Mass: m/z 465 (M + 1), 307, 289, 260, 216, 167, 77. Anal. calcd for $C_{26}H_{19}N_5O_4$: C 67.09, H 4.11, N 15.05, O 13.75; found: C 67.05, H 4.08, N 15.04, O 13.73.

2.3.6 Synthesis of 5-((*Z*)-1-{4-[4-(2,4-dioxo-1,3-thiazolan-5-ylidenmethyl)(phenyl)anilino]phenyl}methylidene)-1,3-thiazolane-2,4-dione (DT). DT was synthesized by the same procedure as **DH**, affording an orange coloured solid in 86.6% yield. m.p.: 246–248 °C. FT-IR (cm^{-1}): 3459, 1733, 2921, 1683, 1580, 1503, 1329, 1284, 1185, 1147, 685, 645. ^{1}H NMR (DMSO-d_6, 400 MHz): δ (ppm): 12.01 (s, 2H), 7.71 (s, 2H), 7.52 (d, J = 8.0 Hz, 4H), 7.41 (t, J = 8.0 Hz, 2H), 7.24 (t, J = 8.0 Hz, 1H), 7.16 (d, J = 8.0 Hz, 2H), 7.10 (d, J = 8.0 Hz, 4H). ^{13}C NMR (DMSO-d_6, 100 MHz): 168.4, 168.0, 148.5, 145.8, 132.3, 131.7, 130.7, 127.8, 127.0, 126.2, 123.4, 121.5. Mass: m/z = 499 (M + 1), 91, 66, 43. Anal. calcd for $C_{26}H_{17}N_3O_4S_2$: C 62.51, H 3.43, N 8.41, O 12.81, S 12.84; found: C 62.46, H 3.39, N 8.38, O 12.79, S 12.82.

2.4 Preparation of TiO_2 electrode

The TiO_2 electrode was prepared according to a reported literature procedure.[33] An amount of acetic acid (12 g, 0.2 mol) was added all at once to 58.6 mg (0.2 mol) of titanium isopropoxide under stirring at room temperature. The modified precursor was stirred for about 15 min and poured into 290 mL of water as quickly as possible with vigorous stirring (700 rpm). A white precipitate was instantaneously formed. One hour of stirring was required to achieve a complete hydrolysis reaction. After adding 4 mL of concentrated nitric acid, the mixture was heated from room temperature to 80 °C within 40 min and peptized for 75 min. Water was then added to the cooling liquid mixture to adjust the volume to a final 370 mL. The resulting mixture was kept in a 570 mL titanium autoclave and heated at 250 °C for 12 h. Following this step, 2.4 mL of 65% nitric acid was added and the dispersion was treated with a 200 W ultrasonic titanium probe at a frequency of 30 pulses every 2 s. The resultant colloidal solution was concentrated with a rotary evaporator to contain 13 wt% TiO_2. Finally, it was triply centrifuged to remove nitric acid and washed with ethanol three times to produce a white precipitate containing 40 wt% TiO_2 in ethanol and only trace amounts of water.

2.5 Fabrication of DSSCs

All the anode films for the DSSCs were made under the same standard conditions[33] and are composed of a 12 mm thick transparent layer (TiO_2 with diameter of 20 nm) and a 6 mm thick scattering layer (TiO_2 nanoparticles with a diameter of 200 nm). Specifically, a doctor blade technique was utilized to prepare the photoanode (TiO_2) films. Then, the electrodes were immersed in a 0.3 mM dye bath in acetonitrile : *t*-butanol (volume ratio, 1 : 1) solution for these dyes and maintained in the dark for 18 h. Afterward, the electrodes were rinsed with ethanol to remove non-adsorbed dyes and dried in air. To prepare the counter electrode, Pt catalyst was deposited on cleaned FTO glass by coating with a drop of H_2PtCl_6 solution (10 mM in 2-propanol solution) with heat treatment at 400 °C for 15 min. The dye-containing TiO_2 electrode and Pt counter electrode were assembled into a sandwich-type cell. The devices were completed by filling the electrolyte by pre-drilled holes in the counter electrodes and finally the holes were sealed with a Surlyn sheet and a thin glass cover by heating.

2.6 Photovoltaic performance measurements

Current density–voltage measurements were performed using simulated AM 1.5 sunlight with an output power of 100 mW cm^{-2}. Electrochemical impedance spectroscopy (EIS), was measured in

the frequency range of 10^{-1}–10^{5} Hz under 1 sun bias illumination under open circuit conditions using computer controlled potentiostat/galvanostat (IVIUM, Compactstat). Incident photon-to-current efficiencies (IPCE) were measured with monochromatic incident light of 1×10^{16} photon per cm^2 under 100 mW cm^{-2} with bias light in DC mode (Jarrel Ash monochromator, using a 100 W halogen lamp). A calibrated photodiode (Thorlabs) was used to study the optical properties of layers.

2.7 Theoretical calculation methods

The electronic configuration and geometric structure of the dyes were optimized by density functional theory (DFT) calculations with the Gaussian 03 program package at the B3LYP/6-31G(d,p) level of theory. To model the adsorption modes of the dyes on the TiO_2 anatase(101) surface, periodic density functional theory calculations were carried out using the Dmol^3 package as implemented in Material Studio (version 5.5). The TiO_2 anatase(101) surface is modelled using a slab with a thickness of six atomic layers. Periodic boundary conditions are employed with a surface supercell of 21.77 × 15.10 Å^2 and a vacuum layer of at least 20 Å to prevent interaction between adjacent slabs. For these calculations, we used the generalized gradient approximation (GGA) functional with Perdew and Wang (PW91) formulation. The electronic properties of core electrons were treated with DFT semi-core pseudoplots in term of the DNP basis set. The convergence energy tolerance, gradient, and displacement convergence were 1.0×10^{-5} Ha, 0.004 Ha Å^{-1}, and 0.005 respectively.

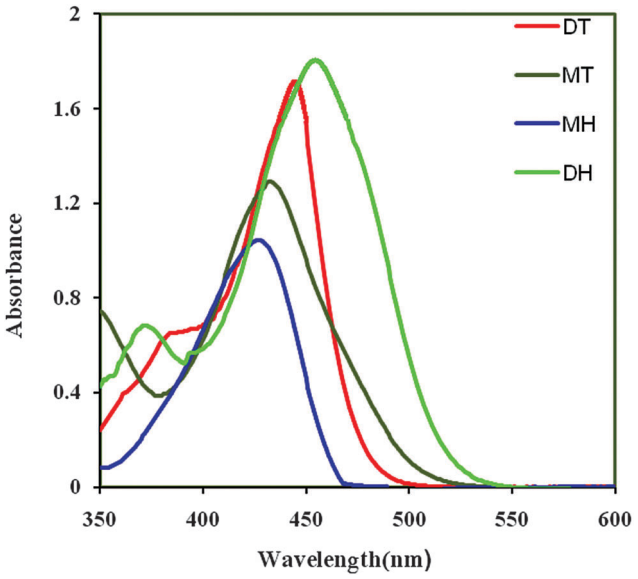

Fig. 2 Absorption spectra of the organic dyes in THF solution.

3. Results and discussion

3.1 Optical properties

The UV-vis absorption spectra of sensitizers **MH**, **MT**, **DH** and **DT** are shown in Fig. 2, and their photophysical data are listed in Table 1. In general, D–π–A organic dyes show two principal groups of absorption bands: one due to intramolecular charge transfer (ICT) transitions in the visible region and the other due to localized π–π* transitions at shorter wavelengths.[34] The two dyes, **MT** and **MH**, exhibit one visible absorption band that appears at 427 and 433 nm, respectively, which can be ascribed to an efficient charge-separated state produced by an intramolecular charge transfer (ICT) between the donor and acceptor end groups.

As can be seen in Fig. 2, **DT** and **DH** exhibit obvious maximum absorption peaks at two distinct regions. The higher energy peaks at 385 nm for **DT** and at 374 nm for **DH** can be ascribed to a π–π* transition of the triphenylamine unit and the lower energy peaks at 446 nm for **DT** and at 457 nm for **DH** can be attributed to the intramolecular charge transfer (ICT) between the arylamine donating unit and acceptor/anchoring moiety, thereby producing an efficient charge separated state.[35] The molar extinction coefficients (ε) of the ICT bands of **MH**, **MT**, **DH** and **DT** were 3.37×10^4, 4.31×10^4, 5.91×10^4 and 6.10×10^4 M^{-1} cm^{-1}, respectively (Table 1) which are higher than that of the standard N719 sensitizer (1.42×10^4 M^{-1} cm^{-1}),[36] indicating a better light harvesting ability of these new triphenylamine based metal-free organic dyes than that of classical organometallic dyes. The higher value of ε for **DH** and **DT** is due to the extended conjugation with π linker units and two anchoring units. An increased number of anchoring units leads to a higher ε value due to the large oscillator strength of the charge transfer transition, according to the Franck–Condon principle.[37]

The absorption spectra of triphenylamine dyes adsorbed on the TiO_2 surface are shown in Fig. 3 and the corresponding data are included in Table 1. When the dyes were attached on TiO_2 films, the absorption spectra may shift more or less compared with those in solution because of strong interactions between the dyes and semiconductor surface, which can lead to aggregates

Table 1 Band gap (calculated by DFT/B3LYP), absorption, and electrochemical parameters for organic dyes

Dye	(HOMO/LUMO)[a] (eV)	Band gap[a]	(λ_{abs}[b]/nm)/ (ε/10^4 M^{-1} cm^{-1})	λ_{max}[c]/nm	λ_{max}[c]/nm	HOMO[d] (*vs.* NHE) (V)	E_{0-0}[e] (eV)	LUMO[f] (*vs.* NHE) (V)
MH	−4.82/−2.81	2.01	427 (3.37)	398	398	1.57	2.65	−1.08
MT	−5.00/−3.05	1.95	433 (4.31)	395	395	1.70	2.53	−0.83
DH	−4.92/−3.13	1.79	457 (5.91)	410	410	1.45	2.39	−0.94
DT	−5.20/−3.49	1.71	446 (6.10)	408	408	1.46	2.43	−0.97

[a] B3LYP/6-31G(d) calculated values. [b] Absorptions of charge-transfer transition were measured in THF; ε: molar extinction coefficient at λ_{max}. [c] Maximum absorption on TiO_2 films. [d] HOMO of dyes measured by cyclic voltammetry in 0.1 M tetrabutylammonium hexafluorophosphate in acetonitrile. [e] E_{0-0} = 1240/λ intersection. [f] LUMO was calculated by HOMO−E_{0-0}.

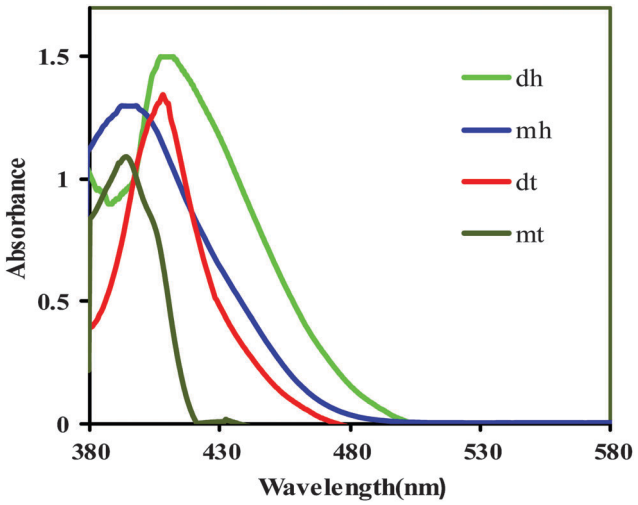

Fig. 3 Absorption spectra of the four dyes absorbed on TiO_2 film electrodes.

of the dyes forming on the semiconductor surface, such as H-aggregation for the blue shift or J-aggregation for the red shift. The absorption spectra on TiO_2 are broadened and the maximal absorption peaks for **MH**, **MT**, **DH** and **DT** on the TiO_2 film are observed at 398, 395, 410, and 408 nm, respectively. They are blue shifted by 29, 38, 36, and 49 nm compared with the solution spectra, respectively. This is ascribed to deprotonation of the dyes or the formation of H-aggregation on the semiconductor surface.[38] Hypsochromic shifts on the TiO_2 surface were assigned to the interaction of the anchoring group with the surface which directly reduces the energy of the π^* level and the formation of H-aggregates on the TiO_2 surface.[39,40] Thus, a difference in the number and type of anchoring groups in the dyes may result in different arrangement of the dyes on the TiO_2 surface.

3.2 Electrochemical properties

Cyclic voltammetry in MeCN solution was used to determine the highest occupied molecular orbital (HOMO) and lowest unoccupied molecular orbital (LUMO) of the dyes. The relevant CV data are presented in Table 1. The results are presented in Fig. 4 and graphically depicted in Fig. 5.

To evaluate the mechanism of electron transfer and the reduction of the dye cation back to its original state for the next cycle, cyclic voltammograms were recorded in acetonitrile solution containing tetrabutylammonium hexafluorophosphate (0.1 M) as the supporting electrolyte, TiO_2 films stained with sensitizer as the working electrode and Pt as the counter electrode with a scan rate of 100 mV s^{-1}. The potentials measured *vs.* Fc/Fc^+ was converted into normal hydrogen electrode (NHE) potentials.[41]

The ground oxidation potentials (E_{ox}) correspond to the highest occupied molecular orbitals (HOMO) while the lowest unoccupied molecular orbitals (LUMO) were obtained from the values of E_{ox} and the zero–zero band gaps (E_{0-0}) estimated from the onset of the UV-visible absorption spectra. The HOMO and LUMO levels of the dyes are collected in Table 1. Apparently, the HOMO levels of all dye molecules are lower than the iodide/triiodide redox potential value (0.4 V *vs.* NHE), indicating that the oxidized dyes could be efficiently regenerated by the electrolyte. Their LUMO levels are estimated from the HOMOs

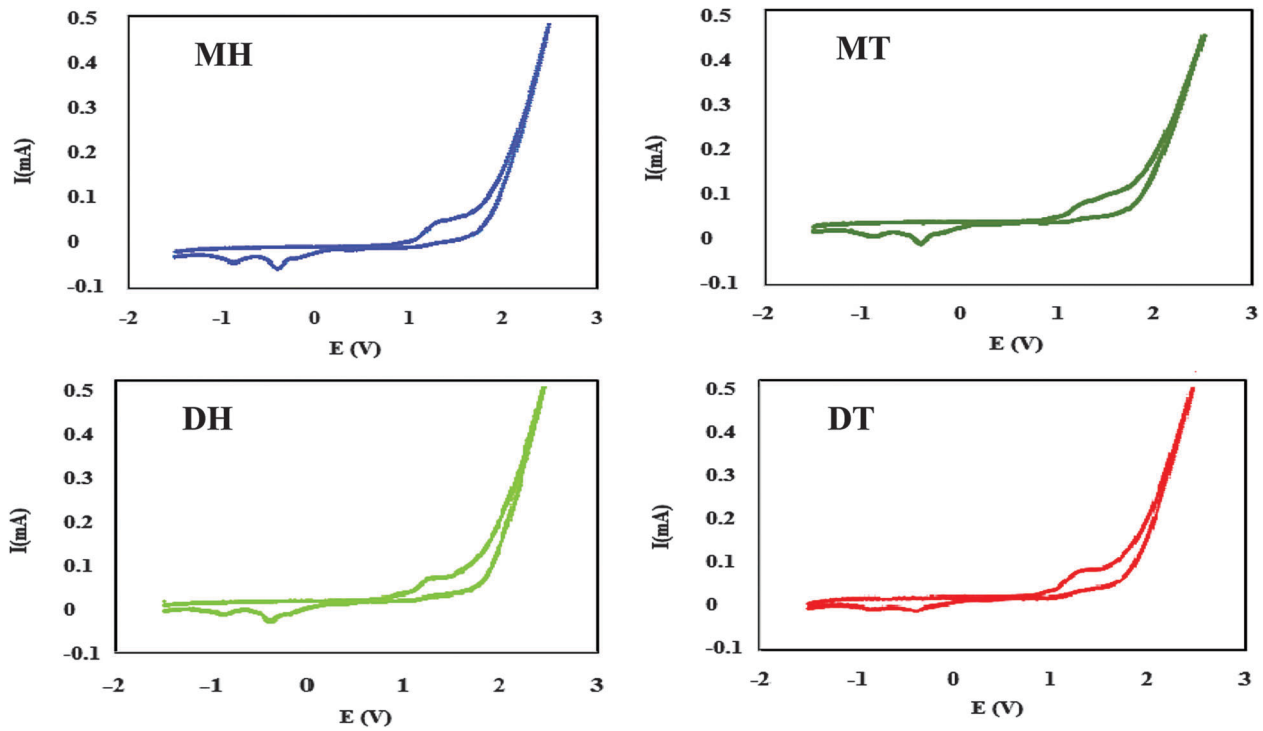

Fig. 4 Cyclic voltammograms of the four dyes.

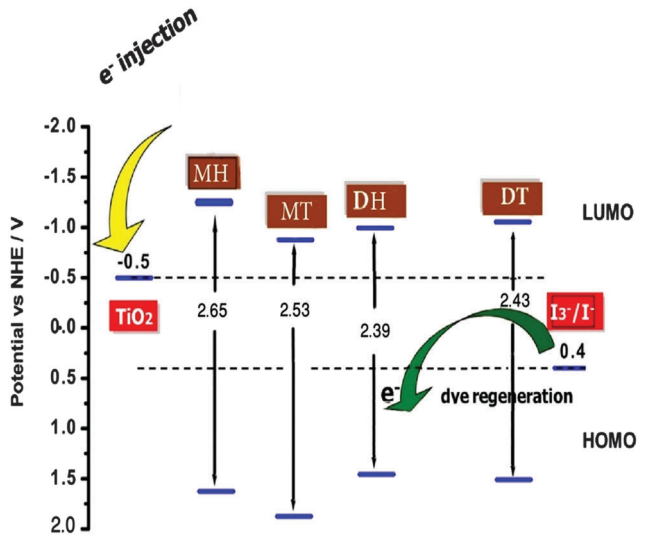

Fig. 5 The schematic energy levels of **MH**, **MT**, **DH** and **DT** based on absorption and electrochemical data.

and the energy gaps (E_{0-0}), and the values are higher than the conduction band (CB) of the TiO_2 anode (0.5 V *vs.* NHE), suggesting an efficient driving force for electron injection from the LUMO of the dyes to the CB band of TiO_2 semiconductor. The LUMO level order of the di-anchoring dyes was different from those of mono-anchoring dyes possibly due to the conjugation length and the electron withdrawing nature of the acceptor of the synthesized dyes. Consequently, although the additional anchoring group makes the HOMO level of the di-anchoring group slightly more positive, the HOMO–LUMO gap decreased and the absorption spectra were red-shifted. Therefore, the four dyes are feasible for application in DSSCs.

3.3 Molecular orbital calculations

To gain further insight into the distinct difference in the photovoltaic performance of these dyes, DFT calculations were carried out at the B3LYP/6-31G(d) level for the geometry optimization and the calculated results are displayed in Table 1. As shown in Fig. 6, the HOMO orbitals of four dyes are delocalized throughout the whole structure, and the LUMO orbital is mainly located at the linker and extends through the anchoring unit. Obviously, the HOMO and LUMO perfectly show the donor–acceptor character of the triphenylamine and anchoring groups. The availability of sufficient electron density at the anchoring group in the LUMO results in good electronic coupling between the excited electrons of the sensitizer in the LUMO with the vacant d-orbitals of TiO_2 where they are attached to fabricate the photoanode. This indicates facile intramolecular charge separation in these molecules and results in facile electron injection after photoexcitation. In the case of **MH** and **DH** dyes, the LUMO levels were majorly distributed in the hydantoin moiety. This is because of the strong electron withdrawing nature of the N atom compared with the S atom in thiazolidinedione. It is suggested that the N atom increases the electron withdrawing nature of the hydantoin which also induces intramolecular charge transfer from the donor to the acceptor group under illumination compared with thiazolidinedione.

The results indicated that the HOMO–LUMO excitation induced by light irradiation can effectively move the electron distribution from the TPA moiety to the 2,4-thiazolidinedione/hydantoin moiety. Photoinduced electrons can be efficiently transferred from the dye to the TiO_2 surface by this electron separation.

3.4 Photovoltaic device performance

Fig. 7 shows the current density–voltage (J–V) characteristics of solar devices based on the four dyes. Photovoltaic parameters including the short circuit photocurrent density (J_{sc}), open circuit voltage (V_{oc}), fill factors (FF) and power conversion efficiency (PCE) are summarized in Table 2. According to Fig. 7, it is clear that the photovoltaic performances of the DSSCs can be clearly affected by the anchoring group in the dye molecules. Power conversion efficiency (PCE) of the DSSCs based on the synthesized dyes increases in the order of **MT** (0.99%) < **DT** (1.42%) < **MH** (1.75%) < **DH** (2.70%). The DSSC based on the **DH** dye shows better properties with an open

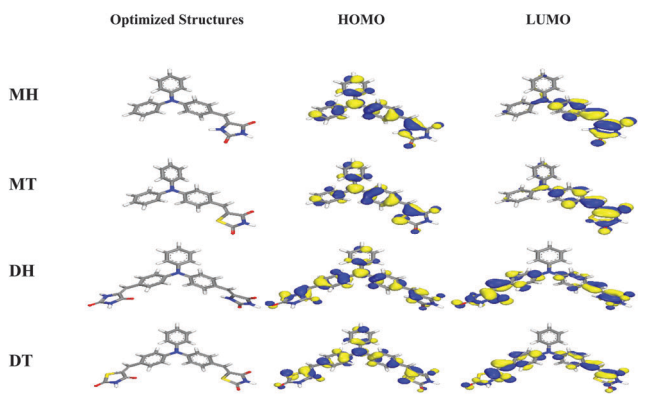

Fig. 6 The frontier molecular orbitals of the HOMO and LUMO levels calculated with B3LYP/6-31G(d) of the synthesized dyes.

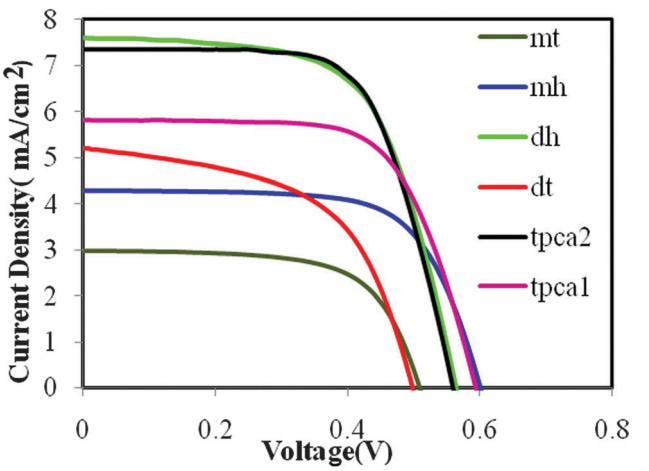

Fig. 7 Photocurrent density *vs.* voltage for DSSCs based on dyes under AM1.5G simulated solar light (100 mW cm^{-2}).

Table 2 The performance parameters of the dye-sensitized solar cells

Dye	J_{SC} (mA cm^{-2})	V_{OC} (V)	FF	PCE (%)
MH	4.29	0.60	0.67	1.75
MT	2.98	0.51	0.65	0.99
DH	7.60	0.57	0.62	2.70
DT	5.19	0.50	0.55	1.42
TPAC1	5.81	0.59	0.68	2.31
TPAC2	7.34	0.56	0.67	2.73

circuit voltage of 0.57 V, a short circuit photocurrent density of 7.60 mA cm^{-2} and a fill factor of 0.62 corresponding to an overall light to electricity conversion efficiency of 2.70%, which is observable in Fig. 7.

The J_{sc} of the DSSCs increased in the order of **MT** < **MH** < **DT** < **DH**. Double anchoring units in the dye are favorable for electron injection and hence photocurrent generation. The J_{sc} is related to the molar extinction coefficient of the dye molecule, in which a higher molar extinction coefficient has a better light harvesting ability and yields a higher J_{sc}. **DH** has the highest light harvesting efficiency and consequently an improved J_{sc} (7.60 mA cm^{-2}) due to its largest molar extinction coefficient, broader absorption spectrum and highest IPCE value among all the dyes.

The increased J_{sc} value of **DH** compared with other three dyes mainly derives from its relatively better light harvesting ability (broad absorption spectrum and high molar extinction coefficient) which is reflected in its better IPCE spectrum.

V_{oc} values increased in the order of **DT** < **MT** < **DH** < **MH**. The cells fabricated with the di-anchoring dyes showed lower V_{oc} values compared to those with the mono-anchoring dyes.

For both **DT** and **DH** dyes, the V_{oc} decreases slightly with the increase of the conjugation length compared to those with the mono-anchoring dyes.

The performance of triphenylamine based sensitizer **TPAC1** and **TPAC2** with 2-cyanoacetic acid acceptor were also investigated under the same conditions for comparison. The results are shown in Fig. 7. Under the same conditions, the **TPAC1** and **TPAC2** sensitized cells gave J_{sc} values of 5.81 and 7.34 mA cm^{-2}, V_{oc} of 0.59 and 0.56 V and FF of 0.68 and 0.67, corresponding to η values of 2.31% and 2.73%, respectively. The results for **TPAC1** and **TPAC2** are comparable to the literature reported values. For example, in 2008, **TPAC1** was reported to show a η of 2.47% and in 2008 and 2014, the efficiency of **TPAC2** was reported to be 3.01 and 2.86%, respectively.[42,43] Comparing the performances of **TPAC2** with four dyes, apparently 2-cyanoacetic acid could enhance the power conversion efficiency, which is mainly attributed from the J_{sc} values. The results indicate that the more dye that is adsorbed on the TiO_2 surface, the better J_{sc} that is observed. The cell fabricated with the dianchoring dye **TPAC2** showed lower V_{oc} values compared to those with the mono-anchoring dye **TPAC1**. The dianchoring dyes transfer more protons to the TiO_2 surface upon adsorption.[44] Thus, the high concentration of the protons changes the TiO_2 surface to a more positive state, lowering the conduction band edges of TiO_2 and lowering V_{oc}.[45,46]

Fig. 8 plots the incident photon-to-electron conversion efficiencies (IPCE) which are functions of the incident wavelength for the corresponding DSSCs of the resulting organic dyes on TiO_2 films. It should be noted that the IPCE values increase in the order of **DT** < **MT**< **MH** < **DH**. The onset of IPCE for the **DH** device was *ca.* 700 nm. IPCE values higher than 90% were observed in the range of 430–520 nm with a maximum value of 95% at 480 nm for the device based on **DH**, while **MH** showed about 78% at 400 nm. The IPCE spectra of the DSSC based on **MT** is slightly lower than that of the DSSC based on **MH**. However, the IPCE spectrum of **DT** is much lower, with a maximum IPCE of 36% at 470 nm.

The relatively higher maximum IPCE for **DH** compared with the other three dyes is well in agreement with the tendency of

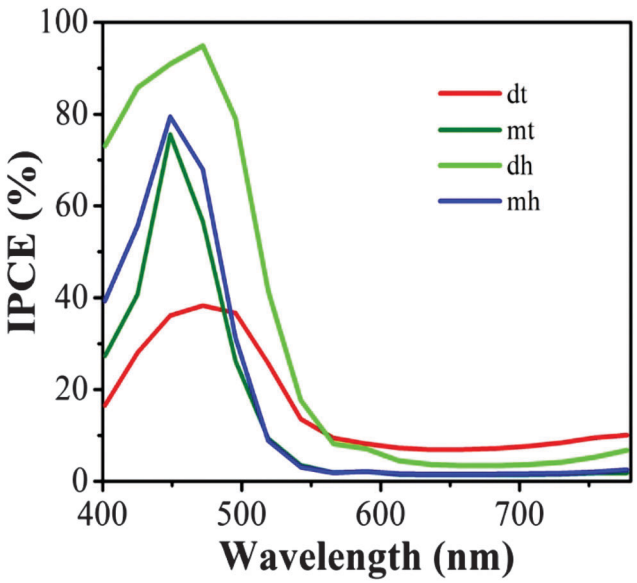

Fig. 8 IPCE spectra of **MH**, **MT**, **DH** and **DT**.

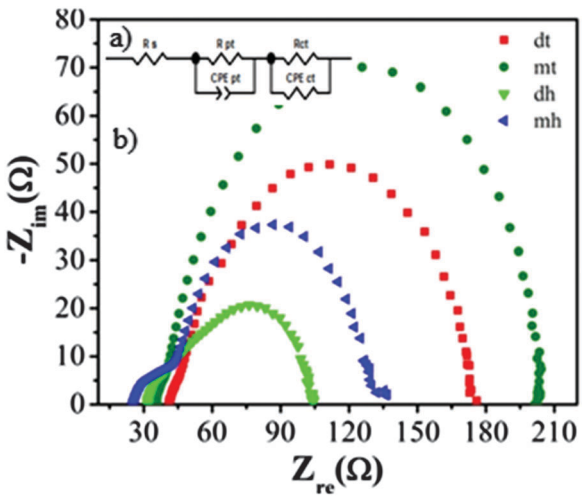

Fig. 9 Electrochemical impedance spectra ((a) Nyquist plot and (b) equivalent circuit for (a)) of DSSCs for the four dyes.

UV-vis absorption properties. IPCE spectra of the cells with the di-anchoring dyes are broader than those with mono-anchoring dyes, promoting higher J_{sc} values. This result indicates that the di-anchoring dyes with broad and red-shifted spectra could inject more electrons.

Fig. 9 shows the electrochemical impedance spectroscopic (EIS) analysis of the cells which were recorded using a set up whose equivalent circuit is presented in Fig. 9(b). The results of EIS data fitting are listed in Table 3. R_{ct}, τ and C_{μ} correspond to the charge transfer process occurring at the TiO_2/dye/electrolyte interface, electron life time and chemical capacitance, respectively. CPE ct-T and CPE ct-P are the parameters of constant phase element charge transfer (CPE ct).

Table 3 EIS parameters obtained from modelling the EIS results

Dye	R_{ct} (Ω cm^2)	CPE ct-T (10^{-4})	CPE ct-P	τ (ms)	C_{μ} (10^2 μF cm^{-2})
MH	20.38	3.82	0.93	24.38	11.96
MT	41.85	0.50	0.88	4.33	1.03
DH	12.61	3.88	0.80	7.38	5.85
DT	32.02	0.52	0.85	2.87	0.90

Electrochemical impedance spectroscopy (EIS) is performed to elucidate the interfacial charge recombination processes in DSSCs based on the four dyes under dark conditions. The Nyquist plots have two semicircles. The larger semicircle at lower frequencies corresponds to the charge transfer processes at the TiO_2/dye/electrolyte interface, while the smaller semicircle at higher frequencies corresponds to the charge transfer processes at the Pt/electrolyte interface. Specifically, the small circles were almost similar in all dye based DSSCs due to the use of the same counter electrode and electrolyte. On the other hand, there was a substantial difference in the large semicircles, which indicates that charge transfer behavior between TiO_2 and dye or between dye and electrolyte was significantly altered, which is likely due to the surface modifications with different dyes. The charge recombination resistance at the TiO_2 surface, R_{rec}, could be estimated from the radius of the middle semicircle in the Nyquist plot, and the larger R_{rec} meant a slower charge recombination rate. The calculated resistance values (R_{rec}) are 20.38 Ω for **MH**, 42.85 Ω for **MT**, 12.61 Ω for **DH** and 32.02 Ω for **DT**, respectively.

The increased R_{rec} values imply the retardation of charge recombination between the injected electron into the TiO_2 and

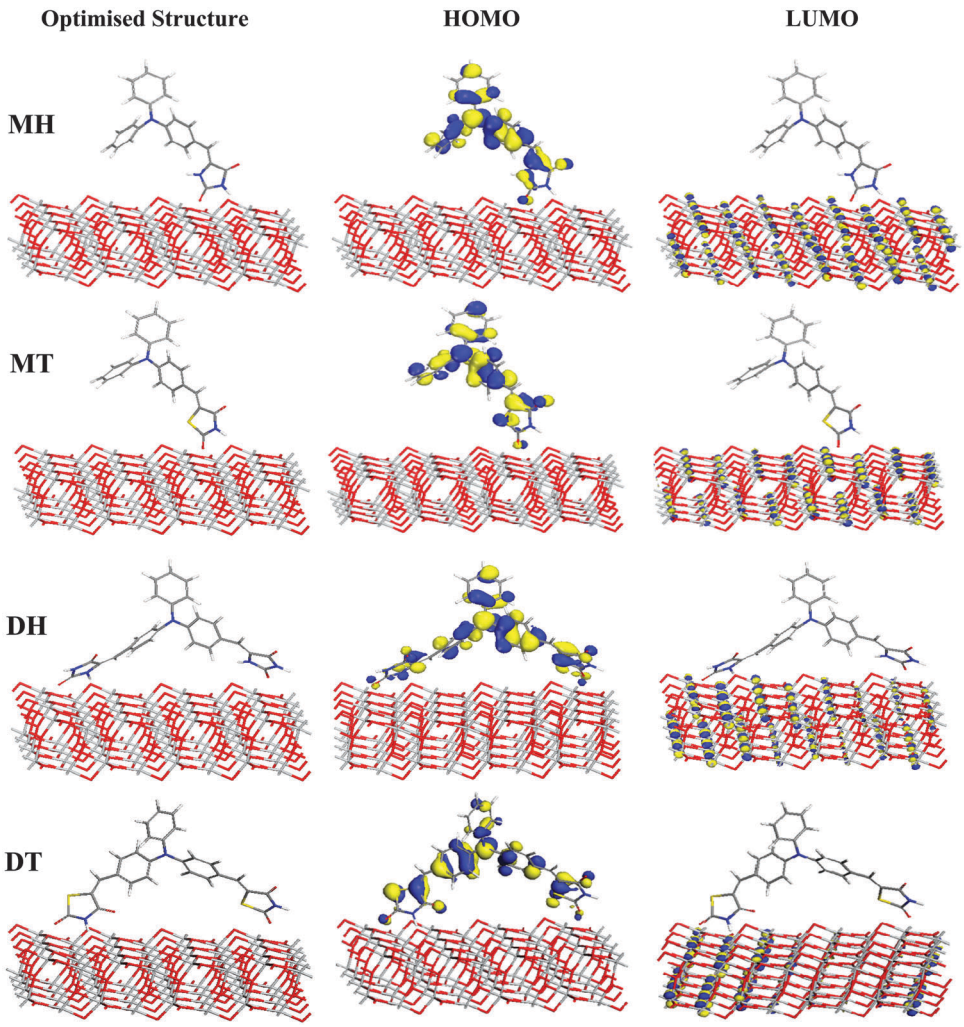

Fig. 10 Frontier orbitals of the dye–TiO_2 complexes.

oxidized species (I_3^-) in the electrolyte, further showing the superiority of the special configuration of **MT**.

By fitting the EIS curves, another important parameter for DSSCs, electron lifetime (τ), could be extracted from the chemical capacitances (C_μ) and R_{CT} using $\tau = C_\mu \times R_{ct}$. The fitted τ increases in the order of **DT** (2.87 ms) < **MT** (4.33 ms) < **DH** (7.38 ms) < **MH** (24.38 ms).

Also, these results obtained from EIS measurements give an explanation for the difference in open circuit voltage for the three dyes. Generally, the influence of dye on V_{OC} has mostly been attributed to electron lifetime, which is related to the tendency of electron recombination in TiO_2 with the I^-/I_3^- redox couple in the electrolyte.[47] The V_{OC} values of the four dyes increase in the order of **DT** (500 mV) < **MT** (510 mV) < **DH** (570 mV) < **MH** (600 mV). The results agree well with the τ values of the devices.

3.5 Adsorption of dyes on TiO_2 anatase(101) surface

The optimized geometries of dye/TiO_2 systems are shown in Fig. 10 and the corresponding bond distances as well as adsorption energies are provided in Table 4. As shown in Table 4, all the dyes show a rather strong adsorption onto the TiO_2 surface, with binding distances of 2.13, 2.15, 2.14–2.15 and 2.32–2.21 Å for **MH**, **MT**, **DH** and **DT**, respectively.

The adsorption energy, E_{ads} is calculated using the expression

$$E_{ads} = E_{(slab+dye)} - E_{slab} - E_{dye}$$

where E_{slab} represents the energy of the clean slab, E_{dye} represents the anchored dye in the gas phase, and $E_{(slab+dye)}$ is the total energy of the complex of the slab with anchored dye. A negative value of $E_{ads} < 0$ indicates stable adsorption. As shown in Table 4, the adsorption energy (E_{ads}) of each dye/TiO_2 complex was calculated to be −1.94, −0.90, −2.82 and −1.43 eV for **MH**, **MT**, **DH** and **DT**, respectively, which are sufficiently large to allow the assumption that the dye molecules are chemisorbed on the surface of TiO_2.

The HOMOs and LUMOs of dye–TiO_2 complexes were also studied. There was electron distribution mostly delocalized on dye molecules in the HOMO, whereas the LUMO showed the injected electron delocalized dominantly on TiO_2 surface. These results indicate that efficient electron injection from the LUMO of dyes to the CB of TiO_2 substrate can be performed through hydantoin/2,4-thiazolidinedione acceptor groups, which implies that intermolecular charge transfer (CT) transition between dye and TiO_2 occurred. These results show that direct charge transfer is the dominant mechanism for the charge-injection process within the dye–TiO_2 complex.

Table 4 Selected bond lengths (Å) and adsorption energies (eV) of dye/TiO_2 systems

	Ti–O (Å)	Ti–O (Å)	E_{ads} (eV)
MH–TiO_2	2.13	—	−1.94
MT–TiO_2	2.15	—	−0.90
DH–TiO_2	2.14	2.15	−2.82
DT–TiO_2	2.32	2.21	−1.43

4. Conclusion

In conclusion, we have demonstrated a design strategy and synthesis of novel D–π–A type organic sensitizers, in which triphenylamine dyes are utilized as the donor and 2,4-thiazolidinedione/hydantoin as the acceptor. The influence of different anchoring groups on the photophysical, electrochemical, and photovoltaic properties was studied. Computational and experimental results support that electron transfer from the rich π-system of the donor group to the acceptor side could give good spectral response and cell efficiency in dye sensitized solar cell devices.

The introduction of the additional anchoring group extended the conjugation of the dyes, leading to red-shifting of their absorption spectra. The di-anchoring dyes transferred more electrons to the TiO_2 electrode, increasing the J_{sc} value. On the other hand, the di-anchoring dyes transferred more protons to TiO_2. This lowered the Fermi level of the TiO_2 and the V_{oc} of the cells. As a result, the dye containing two hydantoin acceptor unit delivers the best performance among the dyes studied, exhibiting a power conversion efficiency of 2.70%, with J_{sc} of 7.60 mA cm^{-2} and V_{oc} of 570 mV under simulated AM 1.5 irradiation (100 mW cm^{-2}).

This result indicates that compared to 2,4-thiazolidinedione and hydantoin as an acceptor/anchor, a triphenylamine and hydantoin based device opens up a new avenue for researchers towards dye sensitized solar cells.

Acknowledgements

We would like to thank Yasouj University for the financial support (Research Council Grant).

References

1 C.-H. Chen, Y.-C. Hsu, H.-H. Chou, K. R. J. Thomas, J. T. Lin and C.-P. Hsu, *Chem. – Eur. J.*, 2010, **16**, 3184–3193.
2 B. O'Regan and M. Gratzel, *Nature*, 1991, **353**, 737–740.
3 Y. Çakmak, S. Kolemen, M. Buyuktemiz, Y. Dedeb and S. Erten-Ela, *New J. Chem.*, 2015, **39**, 4086–4092.
4 H. Jia, K. Shen, X. Ju, M. Zhang and H. Zheng, *New J. Chem.*, 2016, **40**, 2799–2805.
5 Y. Wang, L. Xu, X. Wei, X. Li, H. Ågren, W. Wu and Y. Xie, *New J. Chem.*, 2014, **38**, 3227–3235.
6 S. Mathew, A. Yella, P. Gao, R. H. Baker, B. F. E. Curchod, N. A. Astani, I. Tavernelli, U. Rothlisberger, Md. K. Nazeeruddin and M. Grätzel, *Nat. Chem.*, 2014, **6**, 242–247.
7 W. Zeng, Y. Cao, Y. Bai, Y. Wang, Y. Shi, M. Zhang, F. Wang, C. Pan and P. Wang, *Chem. Mater.*, 2010, **22**, 1915–1925.
8 (*a*) S. Haid, M. Marszalek, A. Mishra, M. Wielopolski, J. Teuscher, J. E. Moser, R. Humphry-Baker, S. M. Zakeeruddin, M. Grätzel and P. Baeuerle, *Adv. Funct. Mater.*, 2012, **22**, 1291–1302; (*b*) M. F. Xu, M. Zhang, M. Pastore, R. Z. Li, F. De Angelis and P. Wang, *Chem. Sci.*, 2012, **3**, 976–983; (*c*) P. Ganesan, A. Chandiran, P. Gao, R. Rajalingam, M. Grätzel and M. K. Nazeeruddin, *J. Phys. Chem. C*, 2014, **118**, 16896–16903; (*d*) K. Pei, Y. Z. Wu,

W. J. Wu, Q. Zhang, B. Q. Chen, H. Tian and W. H. Zhu, *Chem. – Eur. J.*, 2012, **18**, 8190–8200.
9 K. Hara, T. Sato, R. Katoh, A. Furube, Y. Ohga, A. Shinpo, S. Suga, K. Sayama, H. Sugihara and H. Arakawa, *J. Phys. Chem. B*, 2003, **107**, 597–606.
10 Z.-S. Wang, Y. Cui, K. Hara, Y. Dan-oh, C. Kasada and A. Shinpo, *Adv. Mater.*, 2007, **19**, 1138–1141.
11 Z.-S. Wang, Y. Cui, Y. Dan-oh, C. Kasada, A. Shinpo and K. Hara, *J. Phys. Chem. C*, 2007, **111**, 7224–7230.
12 R. Chen, X. Yang, H. Tian and L. Sun, *J. Photochem. Photobiol., A*, 2007, **189**, 295–300.
13 R. Chen, X. Yang, H. Tian, X. Wang, A. Hagfeldt and L. Sun, *Chem. Mater.*, 2007, **19**, 4007–4015.
14 K. Sayama, S. Tsukagoshi, K. Hara, Y. Ohga, A. Shinpou, Y. Abe, S. Suga and H. Arakawa, *J. Phys. Chem. B*, 2002, **106**, 1363–1371.
15 K. Sayama, K. Hara, N. Mori, M. Satsuki, S. Suga, S. Tsukagoshi, Y. Abe, H. Sugihara and H. Arakawa, *Chem. Commun.*, 2000, 1173–1174.
16 W.-H. Zhan, W.-J. Wu, J.-l. Hua, Y.-H. Jing, F.-S. Meng and H. Tian, *Tetrahedron Lett.*, 2007, **48**, 2461–2465.
17 X. Ma, J. Hua, W. Wu, Y. Jin, F. Meng, W. Zhan and H. Tian, *Tetrahedron*, 2008, **64**, 345–350.
18 H. Tian, X. Yang, R. Chen, Y. Pan, L. Li, A. Hagfeldt and L. Sun, *Chem. Commun.*, 2007, 3741–3743.
19 T. Horiuchi, H. Miura, K. Sumioka and S. Uchida, *J. Am. Chem. Soc.*, 2004, **126**, 12218–12219.
20 L. Schmidt-Mende, U. Bach, R. Humphry-Baker, T. Horiuchi, H. Miura, S. Ito, S. Uchida and M. Gratzel, *Adv. Mater.*, 2005, **17**, 813–815.
21 Z.-S. Wang, F.-Y. Li and C.-H. Huang, *J. Phys. Chem. B*, 2001, **105**, 9210–9217.
22 Y.-S. Chen, C. Li, Z.-H. Zeng, W.-B. Wang, X.-S. Wang and B.-W. Zhang, *Mater. Chem.*, 2005, **15**, 1654–1661.
23 W. H. Liu, I. C. Wu, C. H. Lai, C. H. Lai, P. T. Chou, Y. T. Li, C. L. Chen, Y. Y. Hsu and Y. Chi, *Chem. Commun.*, 2008, 5152–5154.
24 S. Haid, M. Marszalek, A. Mishra, M. Wielopolski, J. Teuscher and J. E. Moser, *Adv. Funct. Mater.*, 2012, **22**, 1291–1302.
25 L. L. Tan, H. Y. Chen, L. F. Hao, Y. Shen, L. M. Xiao, J. M. Liu, D. B. Kuang and C. Y. Su, *Phys. Chem. Chem. Phys.*, 2013, **15**, 11909–11917.
26 D. H. Lee, M. J. Lee, H. M. Song, B. J. Song, K. D. Seo, M. Pastore, C. Anselmi, S. Fantacci, F. De Angelis, M. K. Nazeeruddin, M. Grätzel and H. K. Kim, *Dyes Pigm.*, 2011, **91**, 192–198.
27 J. E. Field and D. Venkataraman, *Chem. Mater.*, 2002, **14**, 962–964.
28 B. Hosseinzadeh, A. Salimi Beni, A. Najafi Chermahini, R. Ghahary and A. Teimouri, *Synth. Met.*, 2015, **209**, 1–10.
29 A. Salimi Beni, M. Zarandi, A. R. Madram, Y. Bayat, A. Najafi Chermahini and R. Ghahary, *Electrochim. Acta*, 2015, **186**, 504–511.
30 G. F. Lai, X. R. Bu, J. Santos and E. A. Mintz, *Synlett*, 1997, 1275–1276.
31 S. Ito, T. Murakami, P. Comte, P. Liska, C. Grätzel, M. Nazeeruddin and M. Grätzel, *Thin Solid Films*, 2008, **516**, 4613–4619.
32 Y. Hua, S. Chang, D. Huang, X. Zhou, X. Zhu, J. Zhao, T. Chen, W. Y. Wong and W. K. Wong, *Chem. Mater.*, 2013, **25**, 2146–2153.
33 A. A. Kelkar, N. M. Patil and R. V. Chaudhari, *Tetrahedron Lett.*, 2002, **43**, 7143–7146.
34 Y. Wu, M. Marszalek, S. M. Zakeeruddin, Q. Zhang, H. Tian, M. Grätzel and W. Zhu, *Energy Environ. Sci.*, 2012, **5**, 8261–8272.
35 Z. Ci, X. Yu, M. Bao, C. Wang and T. Ma, *Dyes Pigm.*, 2013, **96**, 619–625.
36 P. Wang, B. Wenger, R. Humphry-Baker, J.-E. Moser, J. Teuscher, W. Kantlehner, J. Mezger, E. V. Stoyanov, S. M. Zakeeruddin and M. Gratzel, *J. Am. Chem. Soc.*, 2005, **127**, 6850–6856.
37 H. Shang, Y. Luo, X. Guo, X. Huang, X. Zhan, K. Jiang and Q. Meng, *Dyes Pigm.*, 2010, **87**, 249–256.
38 P. Shen, X. Liua, S. Jianga, Y. Huanga, L. Yi, B. Zhaoa and S. Tan, *Org. Electron.*, 2011, **12**, 1992–2002.
39 K. Hara, T. Sao, R. Katoh, A. Furube, T. Yoshihara, M. Murai, M. Kurashiga, S. Ito, A. Shinpo, S. Suga and H. Arakawa, *Adv. Funct. Mater.*, 2005, **15**, 246–252.
40 C. J. Qin, A. Islam and L. Han, *Dyes Pigm.*, 2012, **94**, 553–556.
41 Y. Zhao, K. Jiang, W. Xu and D. Zhu, *Tetrahedron*, 2012, **68**, 9113–9118.
42 W. Xu, B. Peng, J. Chen, M. Liang and F. Cai, *J. Phys. Chem. C*, 2008, **112**, 874–880.
43 G. Wu, F. Kong, Y. Zhang, X. Zhang, J. Li, W. Chen, C. Zhang and S. Dai, *Dyes Pigm.*, 2014, **105**, 1–6.
44 M. K. Nazeeruddin, F. De Angelis, S. Fantacci, A. Selloni, G. Viscardi and P. Liska, *J. Am. Chem. Soc.*, 2005, **127**, 16835–16847.
45 Y. S. Yang, H. D. Kim, J.-H. Ryu, K. K. Kim, S. S. Park and K.-S. Ahn, *Synth. Met.*, 2011, **161**, 850–855.
46 H. Shang, Y. Luo, X. Guo, X. Huang, X. Zhan and K. Jiang, *Dyes Pigm.*, 2010, **87**, 249–256.
47 Z. J. Ning, Q. Zhang, H. C. Pei, J. F. Luan, C. G. Lu, Y. P. Cui and H. Tian, *J. Phys. Chem. C*, 2009, **113**, 10307–10313.